ISSN 1063-7826, Semiconductors, 2010, Vol. 44, No. 10, pp. 1342–1348. © Pleiades Publishing, Ltd., 2010.
Original Russian Text © A.Yu. Karlach, G.V. Kuznetsov, S.V. Litvinenko, Yu.S. Milovanov, V.A. Skryshevsky, 2010, published in Fizika i Tekhnika Poluprovodnikov, 2010, Vol. 44, No. 10, pp. 1387–1393.

AMORPHOUS, VITREOUS, POROUS, ORGANIC, AND MICROCRYSTALLINE SEMICONDUCTORS; SEMICONDUCTOR COMPOSITES

The Effect of the Dynamic Adsorption Mode on Impedance of Composite Structures with Porous Silicon

A. Yu. Karlach^, G. V. Kuznetsov, S. V. Litvinenko, Yu. S. Milovanov, and V. A. Skryshevsky

Taras Shevchenko National University of Kyiv, Volodymyrs'ka ul. 64, Kyiv, 01601 Ukraine

^e-mail: karlash@univ.Kiev.ua

Submitted February 17, 2010; accepted for publication March 11, 2010

Abstract—Impedance and optical properties of pressed composites based on microcrystalline and nanoporous silicon powders were studied. Porous silicon crystallites were obtained by stain etching of initial microcrystalline silicon powder. Oxygen passivation of the surface during porous-powder formation provided stability of composite characteristics. An analysis of experimental dependences of the impedance in a frequency range of $1–10^6$ Hz allowed separation of contributions of grain bulk and crystallite interfaces to the total composite conductivity. The results of the study of the time dependences of the impedance were used to determine the variation rates of electrical parameters of composite structures under dynamic adsorption–desorption influence of external reactants (H_2O and C_2H_5OH).

DOI: 10.1134/S1063782610100179

1. INTRODUCTION

Nanocrystalline silicon is a promising material for developing composite structures for optoelectronic converters, gas and chemical sensors, solar panels, and hydrogen accumulators [1–4]. There are several techniques for fabricating ultrafine-grained systems with silicon nanocrystallites: ion doping, pulsed laser deposition, Si cluster deposition in HF discharge plasma, and others. Particular interest is also paid to the development of methods for producing fine-grained ceramic composite structures based on nanoscale silicon powders [5, 6]. The parameters of such structures are easily controlled by varying the initial composition and the properties of the grain bulk (the crystallite structure and sizes, dopant concentrations) and grain boundaries (porosity, the state of crystallites' surfaces) [7–9].

One of the possibilities of modifying the composition and structure of silicon composites may be the use of porous silicon (*por*-Si) powders. The phenomena of energy spectrum quantization, band-gap widening, and permittivity decrease, which are characteristic of nanostructured semiconductors, are observed in *por*-Si monocrystallites. A variety of fractal morphologies of powder material lead to significant differences of electrical, optical, and mechanical characteristics and, hence, to new application possibilities.

Porous silicon *por*-Si powders can be produced using a relatively simple technology of stain etching of fine-grained powder silicon [9, 10]. Methods of stain etching of microcrystalline (*mc*-Si) silicon powder allow the formation of *por*-Si powders with various sizes and morphologies (micro-, nano-, and combined micronanocrystallites). The developed chemically active surface causes high sensitivity of *por*-Si crystallites to various external effects, in particular, to adsorption ones [1, 2]. The problem arises of developing methods providing stability and monitoring of powder *por*-Si parameters at both its production stage and the stage of composite structure formation.

One informative method for revealing the systematic features of the effect of an ambient medium on physicochemical properties of fine-grained composite systems is impedance spectroscopy [11, 12]. Analysis of impedance loci makes it possible to separate the contributions of grain bulk and crystallite interfaces to the conductivity, to study charge transport phenomena, and to clarify the role of adsorption and chemical interaction in various gas and liquid media. As a rule, the frequency dependences of sample capacitive and resistive characteristics are measured under steady-state conditions at fixed parameters of a controlled medium [11]. At the same time, the problem of determining the composite physicochemical state in the dynamic mode in the presence of continuously varying interaction with external reactants remains urgent. The study of temporal transformations of impedance spectra allows a more detailed estimation of the effect of changes in adsorption-induced processes on the sensitivity and dynamics of the response of composite sensor structures.

The objective of this study was to determine the correlations between the frequency and time dependences of the impedance and to determine the variation rate of the parameters of composite structures

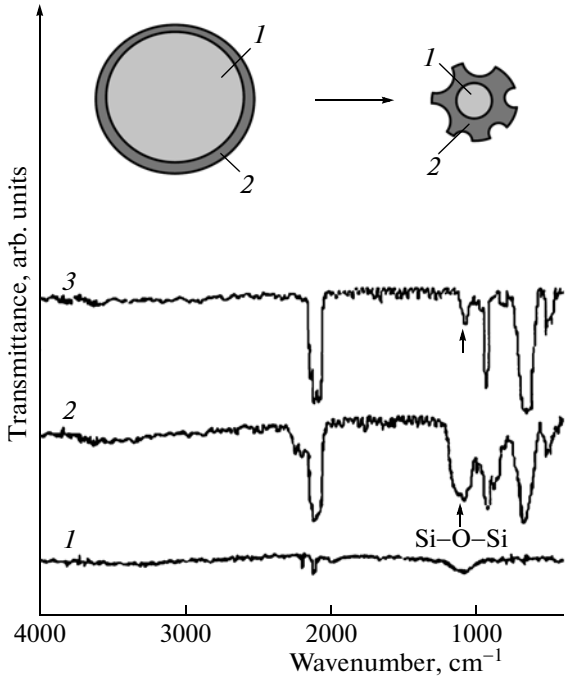

Fig. 1. IR transmission spectra of (*1*) initial microcrystalline silicon powders, (*2*) porous silicon, and (*3*) porous silicon after treatment in a 5% HF solution. The inset shows the schematic change in the crystallite shape before and after chemical etching: (*1*) crystalline core and (*2*) crystallite shell.

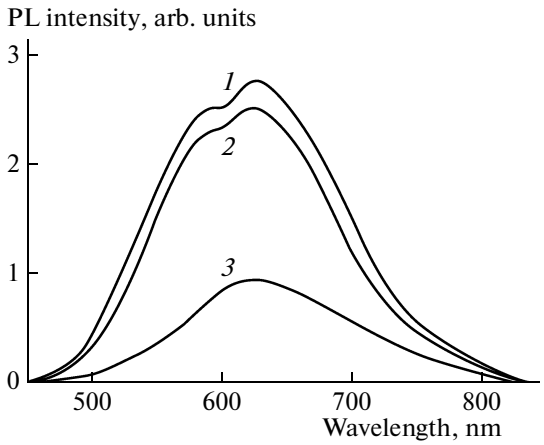

Fig. 2. Effect of compaction ($P = 3 \times 10^7$ Pa) on photoluminescence spectra of porous silicon; (*1*) freshly prepared compacted structure, (*2*) compacted structure after exposure to C_2H_5OH and drying in air, and (*3*) porous silicon (*por*-Si) powder.

with porous silicon directly under conditions of varying adsorption–desorption influence. To study the interaction of composite samples with liquid media, ethanol and water were chosen, the polar molecule adsorption of which results in significant changes in chemical bonds and charge states on the silicon surface [13]. Furthermore, humidity is a necessary component of most gas mixtures monitored using chemical sensors.

2. SAMPLES AND EXPERIMENTAL TECHNIQUE

As an initial material, a fine-grained fraction of commercial *p*-type silicon powder (*mc*-Si) with a resistivity of 0.001–0.003 Ω cm was used. The maximum crystallite size did not exceed several micrometers. The porous silicon powder was prepared by stain etching of the initial powder in a mixture of hydrofluoric and nitric acids ($HF : HNO_3 : H_2O = 4 : 1 : 20$) under continuous stirring at $T = 35$–55°C. After etching, the powder (hereinafter, *por*-Si) was collected in the form of foam and dried in air at room temperature. Such a combined micronanopowder consisted of silicon grains 30–50 nm in size, coated with 2- to 5-nm nanocrystallites (see the inset in Fig. 1). The latter is confirmed by intense red–orange photoluminescence of the porous powder (Fig. 2). The prepared *por*-Si powders were carefully mixed with the initial *mc*-Si powder with weight ratios of 0–100%. The obtained mixtures were pressed in a special mold at pressures as high as 5×10^7 Pa with added Teflon as a binder (to 20 wt %). As a result, sufficiently strong plates shaped as disks 1 mm thick and 10 mm in diameter were obtained. After compaction, composite structures were used for further impedance and optical measurements.

Frequency and time dependences of impedance components were studied using an E7-20 immittance meter in a Teflon cell with pressure contacts (Pt) 10 mm in diameter. The measuring sinusoidal signal amplitude was 40–100 mV, the frequency range was 25–10^6 Hz, and the temperature was 25°C. The measured impedance magnitude $|Z|$ and phase shift angle θ were recalculated to the active $Z_{\mathrm{Re}} = \dfrac{|Z|}{\sqrt{1 + \tan^2\theta}}$ and reactive $Z_{\mathrm{Im}} = |Z|\sqrt{\dfrac{\tan^2\theta}{1 + \tan^2\theta}}$ components of the impedance $Z(\omega) = Z_{\mathrm{Re}} - jZ_{\mathrm{Im}}$. To study the effect of a liquid medium on impedance spectra, the samples were immersed in a cell with distilled water (H_2O) or pure ethanol (C_2H_5OH, 96%). Temporal variations were recorded in the mode of natural drying of the sample after removal of the liquid from the cell volume.

The effect of the conditions of the formation of silicon powders and fine-grained composite structures based on them on transport and recombination processes in the bulk and at grain boundaries was monitored by impedance spectroscopy, IR spectroscopy, and photoluminescence methods. Transmission spectra were measured using a Perkin Elmer Spectrum BXII Fourier spectrometer in the range of 4000–

400 cm^{-1}. The study was performed for both plates and powders in a mixture with KBr. Photoluminescence spectra were studied upon excitation by a pulsed ultraviolet nitrogen laser with wavelength $\lambda = 337$ nm ($\tau =$ 10 ns).

3. EXPERIMENTAL RESULTS AND DISCUSSION

3.1. Initial Powders and Composite Structures

To determine the mechanisms of interaction between the adsorbent and composite structure, the initial composition of silicon powders should be known. Figure 1 shows the results of the study of IR transmission spectra of initial microcrystalline silicon *mc*-Si powders (curve *1*) and porous silicon *por*-Si obtained by stain etching (curve *2*). The inset shows the crystallite shape variation during etching.

The transmission spectra of the initial *mc*-Si powder contain weak vibrational bands (Fig. 1, curve *1*), which is apparently caused by the significant effect of the nonporous crystalline core on the crystallite transparency. The *por*-Si powder prepared by stain etching consists of silicon nanocrystallites with a high concentration of Si–H bonds (Fig. 1, curve *2*). In IR spectra, absorption bands of Si–O (1100 cm^{-1}), SiH_x ($x = 1, 2, 3$) (2080–2140 cm^{-1}), and O_3SiH (2250 cm^{-1}) are identified, which are also characteristic of electrochemically grown porous silicon films [14]. Weak broad absorption bands (3000–3700 cm^{-1}) are typically attributed to the presence of water particles and O–H groups adsorbed on the silicon surface [15, 16]. Water vapor is the basic oxidizing component of ambient air for the Si surface, which, after long standing in air, can cause the formation of absorption bands of O–H groups in Si–OH bonds.

In the case of chemical methods of *por*-Si powder preparation, various mechanisms of dangling bond passivation are possible (by hydrogen and oxygen ions, hydroxyl groups). The probability of substitution of chemically and thermally unstable SiH_x surface groups with more stable silicon–oxygen compounds immediately during formation is controlled by the chemical etchant composition [14, 17]. At low HF solution concentrations, a intense band at a frequency of 1100 cm^{-1} appears in the IR spectrum, which is caused by absorption by Si–O vibrations (Fig. 1, curve *2*). Similar Si–O–Si bridge bonds are observed in silicon dioxide during high-temperature oxidation in dry oxygen [18]. Further porous silicon powder treatment in 5% HF for 20 s results in the expected disappearance of the Si–O band (Fig. 1, curve *3*). The IR spectroscopy data are confirmed by the results of a thermodynamic analysis of electrochemical equilibrium conditions for the interaction of Si with fluoric acid in diluted electrolytes [14]. At low HF concentrations and low pH, the reaction of silicon–oxygen compound formation is thermodynamically more favorable than hydrogen passivation and provides stability of physical and chemical properties of the silicon nanoparticle surface.

During composite structure compaction, silicon nanocrystallites formed on the surface of *por*-Si powder micrograins retain their main physical characteristics. In the photoluminescence spectra of the initial powder and composite in the orange spectral region, a characteristic broad luminescence band is observed, which can be explained by the size effect in structures with different-size oscillators (Fig. 2). The intensity of the luminescence maximum after pressing significantly increases, which seems to be due to efficient formation of bonds between silicon atoms and hydrogen and oxygen atoms adsorbed on the silicon nanoparticle surface. According to [6], an increase in the mechanical pressure during compression of silicon powders results in breaking of Si–Si structural bonds and the appearance of a significant concentration of silicon atom valence bonds, which, during further saturation, form the Si–H and O_y–Si–H_x structures observed in IR spectra (Fig. 1). A decrease in the concentration of dangling bonds with the compaction pressure leads to additional radiative recombination channels and an increase in the intensity of photoluminescence spectrum bands.

After exposure to an ethanol medium, the initial spectrum is almost completely restored in 2–3 h of drying in air (Fig. 2, curve *2*). The compacted structure stability can be controlled by the formation of silicon–oxygen compounds, which are more stable than silicon–hydrogen compounds, on the silicon crystallite surface (Fig. 1). Furthermore, the formation of oxide compounds on the silicon crystallite surface during stain etching prevents particle agglomeration during compaction.

3.2. Frequency Dependences of the Silicon Structure Impedance

Figure 3 shows the frequency dependences of the impedance spectra of composite silicon samples in the complex plane Z_{Re}–Z_{Im} coordinates measured in air. The locus represents either a unit semicircle insignificantly shifted along the Z_{Re} axis (for *mc*-Si + 20% *por*-Si) or dual semicircles (for *mc*-Si). Symbols are the measurement data; solid curves are the results of the approximation using the equivalent circuit (see the inset in Fig. 3).

The impedance $Z(\omega)$ of the equivalent circuit includes the low-frequency R_BC_B and high-frequency R_VC_V circuits corresponding to carrier transport through grain boundaries and in the grain bulk and the ohmic resistance R_0 of current supply contacts [11],

$$Z(\omega) = R_0 + \frac{R_B}{1 + j\omega R_B C_B} + \frac{R_V}{1 + \omega R_V C_V}. \quad (1)$$

For *mc*-Si samples in a frequency range of 1–10^6 Hz, it becomes possible to record two slightly overlapped semicircles in the locus (Fig. 3, curve *2*). This suggests that both crystallite bulk and boundaries contribute to the total structure conductance. At the maximum point at the frequency ω_s, the relations

$$\varpi_s = \frac{1}{\tau_s} = \frac{1}{C_V B_V} \quad \text{and} \quad \varpi_s = \frac{1}{\tau_s} = \frac{1}{C_B B_B}$$

are satisfied for the high- and low-frequency spectral regions, respectively. At $\omega = 0$ and $\omega = \infty$, the imaginary impedance component $Z_{\text{Im}} = 0$, which allows direct determination of the resistances R_0, R_V, and R_B by semicircle positions in the real axis. The parameters of impedance spectrum approximation for *mc*-Si and *mc*-Si + 20% *por*-Si samples are given in Table 1.

As a rule, in fine-grained ceramic materials, the resistivity (per unit length) of crystallite boundaries is much higher than that of the crystallite bulk. However, measured total R_B is smaller than R_V, since grain boundaries can be thinner by several orders of magnitude than the grains themselves. Temperature variations in the resistances R_V and R_B have an activation mechanism; however, they are much less pronounced for the resistance R_V of a heavily doped volume. It is clear that the high doping level of silicon is also a cause of large capacitance C_V. The capacitance C_B inversely proportional to the boundary layer thickness typically does not exceed $C_B = 10^{-9}$ F, whereas it is difficult to characterize the resistance R_B of the intercrystallite layer by a typical value.

In *mc*-Si + 20% *por*-Si samples, *por*-Si clusters existing in the composite make the time constants τ_s of parallel RC circuits of the crystallite bulk and boundaries closer, which results in an increased overlap of the corresponding semicircles. The locus contains only a nonideal unit semicircle (Fig. 3, curve *2*), the actual shape of which is controlled by the degree of overlap of semicircles. In this case, the resistive and capacitive properties of the system are adequately described using a constant phase element (CPE) in the equivalent circuit [12]. After replacing the capacitance with this element, the impedance expression for the composite structure takes the form [11]

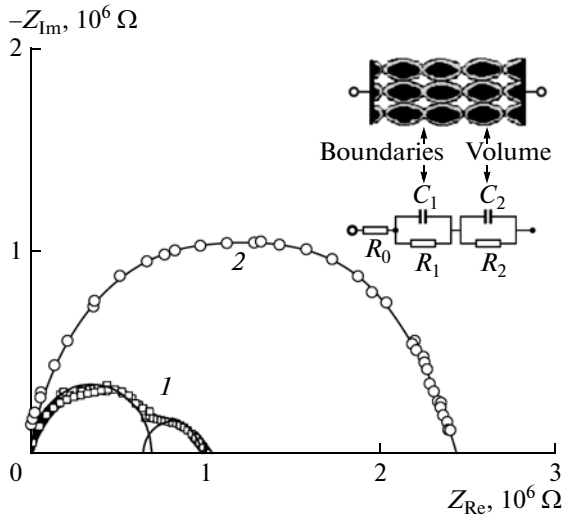

Fig. 3. Dependence of the impedance loci of composite structures on the composition of initial powders for (*1*) *mc*-Si and (*2*) *mc*-Si + 20% *por*-Si. The inset shows the composite structure and the equivalent circuit for modeling.

$$Z(\omega) = R_0 + \frac{R_s}{1 + (j\omega)^s R_s Q}, \qquad (2)$$

where Q is the constant-phase element and s is the exponent characterizing nonuniformity of electrical properties of the structure ($-1 \le s \le 1$). At $s = 1$ and 0, the CPE corresponds to the capacitance and resistance, respectively. The parameters Q, s and resistances R_0, R_s determined for the *mc*-Si + 20% *por*-Si structures are given in Table 1.

The small *por*-Si nanocrystallite sizes cause not only widening of their band gap, but also high electrical resistance irrespective of the carrier concentration in the initial silicon powder [9]. Furthermore, the charge transfer between crystallites is blocked to a large extent by the electrostatic barrier caused by the interface oxide layer.

3.3. Effect of Adsorption on Time Dependences of the Impedance

Let us consider the main features of changes in the impedance spectra of composite structures upon time-varying exposure to an external medium. In the

Table 1

Structure composition	Approximation parameters (*RC*)				
mc-Si	R_B, Ω	C_B, F	R_V, Ω	C_V, F	R_0, Ω
	3.3×10^5	2.5×10^{-10}	6.9×10^5	23.0×10^{-10}	3.9×10^3
	Approximation parameters (CPE)				
mc-Si + 20% *por*-Si	R, Ω	Q	R_0, Ω	s	
	2.4×10^6	5.3×10^{-10}	3.5×10^3	0.87	

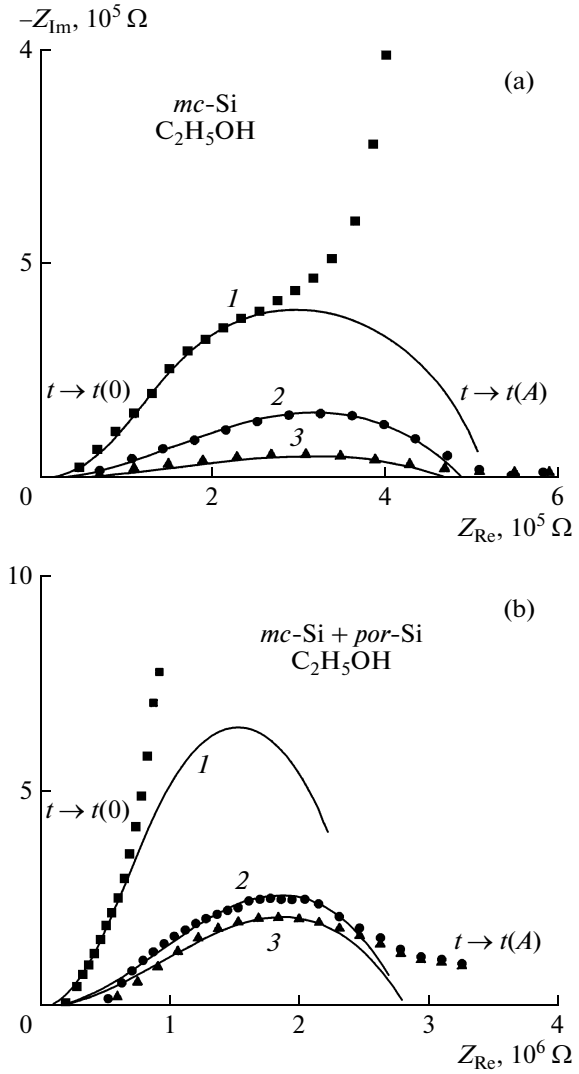

Fig. 4. Modification of impedance loci of (a) *mc*-Si and (b) *mc*-Si + 20% *por*-Si composite structures in a C_2H_5OH (96%) medium at measuring signal frequencies of (*1*) 0.1, (*2*) 1.0, and (*3*) 10 kHz.

impedance measurements at constant frequency ω_n, only resulting values of the series or parallel connected resistance R and capacitance C of the sample are usually obtained, which reflects the entirety of processes in the generalized form. In the case of a parallel RC circuit, the real Z_{Re} and imaginary Z_{Im} parts of the impedance $Z(\omega)$ at fixed frequency ω_n can be written as

$$Z_{Re} = \frac{R}{1+\omega_n^2\tau^2}, \quad -Z_{Im} = \frac{\omega_n\tau R}{1+\omega_n^2\tau^2}, \qquad (3)$$

where $\tau = RC$ is the time constant of the equivalent circuit. It follows from expression (3) that, under the assumption that $R \approx$ const, the dependences of Z_{Re} and Z_{Im} on ω and τ are similar. The impedance spectrum in the complex plane Z_{Re}–Z_{Im} coordinates is described by equation for a circle with coordinates of the center $Z_{Re} = R/2$ and $Z_{Im} = 0$. The dependence maximum is observed at $\tau_n = 1/\varpi_n = C_nR_n$, which allows simple extrapolation of the time dependence of the impedance (R_n and C_n are the resistance and capacitance at the frequency $\omega = \omega_n$). The use of the desorption mode instead of the adsorption mode does not affect the locus shape in the entire τ range ($0 < \tau < \infty$).

At the constant measuring signal frequency $\omega = \omega_n$, the time dependences of the impedance are controlled by the structure resistance and capacitance variations $R(t)$ and $C(t)$. Under the assumption of linear time dependences $R(t)$ and $C(t)$ in the entire range of the adsorbent concentration, we obtain

$$R(t) = R(0)(1+\alpha_R t), \quad C(t) = C(0)(1+\alpha_C t), \quad (4)$$

where

$$\alpha_R = \frac{1}{R(0)}\left[\frac{R(A)-R(0)}{t(A)-t(0)}\right] \quad \text{and}$$

$$\alpha_C = \frac{1}{C(0)}\left[\frac{C(A)-C(0)}{t(A)-t(0)}\right]$$

are, respectively, the $R(t)$ and $C(t)$ variation rates. The indices A and 0 correspond to the adsorption saturation state ("wet" sample) and the state without adsorption ("dry" sample), respectively.

A feature of the studied composite structures is a rather high sensitivity to adsorption–desorption exposure to ethanol and water. Figure 4 shows the effect of the dynamic mode of ethanol desorption on the modification of time dependences of the impedance of the *mc*-Si (Fig. 4a) and *mc*-Si + 20% *por*-Si (Fig. 4b) structures for three frequencies of the measuring signal, $\omega_n = 0.1$, 1, and 10 kHz. Symbols represent experimental data; solid curves correspond to the results calculated according to (3) and (4).

Local electric fields of adsorbed polar molecules cause changes in the surface charge state and electrical parameters of the fine-grained semiconductor structure. Upon drying ($t \longrightarrow t(0)$, "dry" sample), the curves in the complex plane Z_{Re}–Z_{Im} coordinates are shaped as nonideal semicircles in the region of low adsorbate concentrations (Fig. 4). The dependences shaped as semicircles are similar to those obtained from frequency measurements (Fig. 3) and reflect the kinetic nature of charge transport processes. In an ethanol medium ($t \longrightarrow t(A)$, "wet" sample), the transition to the linear dependence is observed in the region of high adsorbate concentrations, which is characteristic of diffusion processes of transport of an electrically active material [12]. Such a dependence may be caused by the relay-race mechanism of ion transport over the surface due to adsorbate wave function overlap [17] at high concentrations of adsorbed ethanol or water molecules. Furthermore, the formation of capillary hydrostatic pressure during precipitation of liq-

Table 2

Structure composition	Parameters					
	α_R, min^{-1}			α_C, min^{-1}		
	10^2, Hz	10^3, Hz	10^4, Hz	10^2, Hz	10^3, Hz	10^4, Hz
mc-Si	0.0096	0.0096	0.0098	1.0	1.70	0.50
mc-Si + 20% *por*-Si	0.0093	0.0093	0.0096	0.80	0.20	0.087

uid in pores can lead to ionic conductivity. The ratio of kinetic and diffusion processes of charge transport is significantly affected by morphological differences between *mc*-Si and *mc*-Si + 20% *por*-Si structures (Fig. 4).

Table 2 lists the calculated variation rates α_R and α_C in composite structures for various measuring signal frequencies.

The room-temperature adsorption sensitivity means that the adsorbate–adsorbent binding energy does not exceed several kT. In this sense, structures with increased *por*-Si concentrations are more stable, since they exhibit lower α_R and α_C in the entire frequency range. The dependence of the impedance on the measurement frequency ω_n is mainly controlled by the contribution of the capacitance component associated with charge state variations.

The kinetics of the surface-charge variation is controlled by the superimposition of two processes: the formation of the surface adsorption charge and recharging of intrinsic surface states of the semiconductor structure under new equilibrium conditions [13]. In the region of higher frequencies $\omega_n > 1$ kHz, charging of relatively fast adsorption states is a dominant factor. The characteristic recharge time depends on the adsorbed dipole concentration and the adsorption–desorption process duration. As a rule, the charge transport rate decreases with the adsorbate concentration, since charging of adsorption states requires overcoming the energy barrier, which becomes higher during adsorption. In the low-frequency region $\omega_n < 1$ kHz, the role of recharging of slower surface states the concentration of which is almost independent of the adsorption process becomes significant. At the same time, changes in the ratio of concentrations of intrinsic and adsorption states and their recharging times can cause the formation of a maximum in the kinetic curve of surface charge variations.

Figure 5 shows the time dependences of the impedance of composite samples of different composition at the frequency $\omega_n = 1$ kHz after exposure to an aqueous medium. The dynamics of water desorption in the drying mode is characterized by lower rates of parameters' variation in comparison with an ethanol medium: $\alpha_R = 0.0067$ min^{-1}, $\alpha_C = 0.15$ min^{-1} for *mc*-Si structures and $\alpha_R = 0.0067$ min^{-1}, $\alpha_C = 0.54$ min^{-1} for *mc*-Si + 20% *por*-Si structures.

In an aqueous medium, the limiting effect of slow diffusion processes manifests itself at lower adsorbate concentrations and lower frequencies. Even at the frequency $\omega_n = 1$ kHz, the locus exhibits the existence of both kinetic (semicircle) and diffusion (straight line) processes (Fig. 5). An increase in the porous silicon content increases the composite structure stability; the parameters of *mc*-Si + *por*-Si composites are almost completely restored after several adsorption–desorption cycles. The kinetic processes of charge transport (semicircle in the locus) are dominant. This is in agreement with the IR spectroscopy data (Fig. 2) on the effect of partial oxygen passivation on a decrease in concentrations of unsaturated valence bonds and charged chemisorbed dipoles on the surfaces of porous silicon nanocrystallites.

A possible cause of the complex mechanism of the current flow through phase interfaces is the low-frequency contribution of ion–proton components (H^+, H_3O^+, OH^-, O^-) caused by the presence of hydrated water in the surface layer of silicon crystallites to the conductance. In the low-frequency spectral region,

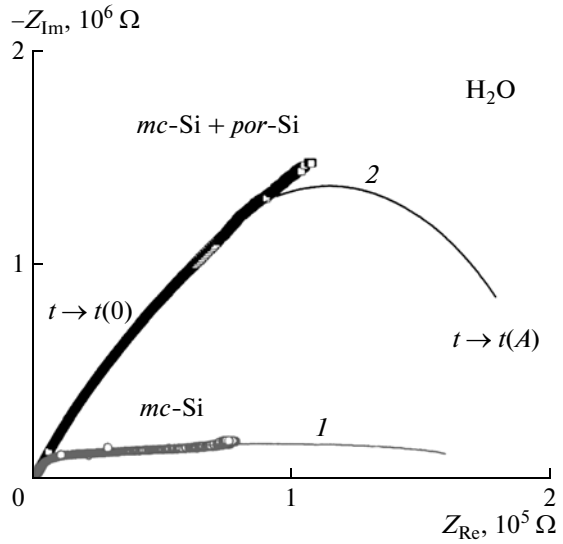

Fig. 5. Modification of impedance loci of (*1*) *mc*-Si and (*2*) *mc*-Si + 20% *por*-Si nanocomposite structures in an H_2O medium at a frequency of 1.0 kHz.

the transport of ion defects in chains of adsorbed water molecules can provide considerable proton conduction in crystalline hydrate compounds the lattice of which is saturated with crystal water [19]. At high frequencies, low-mobility charge components have no time to pass through the phase interface and the intercrystalline layer capacitance becomes frequency independent and is controlled by morphological features of the structure. In the low-frequency region $f < 10^3$ Hz, the frequency-dependent complex component additional to the barrier capacitance should be considered in the graphic-analytical determination of the equivalent circuit parameters.

4. CONCLUSIONS

Thus, we may conclude that graphic-analytical processing of the time dependences of the impedance under conditions of dynamic adsorption makes it possible to obtain information on the crystallite bulk and interface properties in addition to stationary impedance studies in a frequency range.

The differences in the composition and structural characteristics of initial *mc*-Si and *por*-Si powders, as well as in compaction conditions, control the stability of properties of obtained composites. Partial oxygen passivation of the surface immediately upon porous silicon powder formation provides stable characteristics of composite structures. Adsorption of polar molecules (H_2O and C_2H_5OH) controls the kinetics of variations in the surface charge states and, hence, electrical parameters of structures. The results of the study of the time dependences of the impedance allowed determination of the parameter-variation rates for composite structures under conditions of dynamic adsorption–desorption exposure.

ACKNOWLEDGMENTS

The authors are grateful to A. Venrturello and G. Geobaldo (Politecnico di Torino) for letting us have the results of FE-SEM analysis of silicon powders.

REFERENCES

1. M. Y. Channam, A. A. Abouelsaood, and J. F. Nijs, Sol. Energy Mater. Solar Cells **60**, 105 (2000).
2. C. Baratto, G. Faglia, E. Comini. G. Sherveglieri, A. Taroni, V. La Ferrara, L. Quercia, and G. Di Francia, Sens. Actuat. B: Chem. **77**, 62 (2001).
3. V. Strukha, V. Skryshevsky, V. Polishchuk, E. Souteyrand, and J. R. Martin, J. Porous Mater. **7**, 111 (2000).
4. V. A. Skryshevsky, A. Laugier, V. I. Strikha, and V. A. Vikulov, Mater. Sci. Eng. B **40**, 54 (1996).
5. J. Costa, P. Poura, J. K. Morante, and E. Bertran, J. Appl. Phys. **83**, 7879 (1998).
6. N. N. Kononov, G. P. Kuz'min, A. N. Orlov, A. A. Surkov, and O. V. Tikhonevich, Fiz. Tekh. Poluprovodn. **39**, 868 (2005) [Semiconductors **39**, 835 (2005)].
7. É. B. Kaganovich, É. G. Manoilov, I. R. Bazylyuk, and S. V. Svechnikov, Fiz. Tekh. Poluprovodn. **37**, 353 (2003) [Semiconductors **37**, 336 (2003)].
8. S. G. Dorofeev, N. N. Kononov, A. A. Ishchenko, R. B. Vasil'ev, M. A. Gol'dshtrakh, K. V. Zaitseva, V. V. Koltashev, V. G. Plotnichenko, and O. V. Tikhonevich, Fiz. Tekh. Poluprovodn. **43**, 1460 (2009) [Semiconductors **43**, 1420 (2009)].
9. V. Lysenko, J. Vitiello, B. Remaki, D. Barbier, and V. Skryshevsky, Appl, Surf. Sci. **230**, 425 (2004).
10. L. Schirone, G. Sotgiu, and M. Montecchi, J. Luminecs **80**, 163 (1999).
11. A. J. Bard and L. R. Faulkner, *Electrochemical Methods. Fundamentals and Applilcations* (Wiley, New York, 2001).
12. C. Gabrielli, *Used and Application of Electrochemical Impedance Techniques* (Farnborough, 1990).
13. I. V. Gavril'chenko, S. A. Dyachenko, G. V. Kuznetsov, and V. A. Skryshevskii, Ukr. Fiz. Zh. **51**, 460 (2006).
14. S. A. Gavrilov, A. I. Belogorokhov, and L. I. Belogorokhova, Fiz. Tekh. Poluprovodn. **36**, 104 (2002) [Semiconductors **36**, 98 (2002)].
15. R. A. Bley, S. M. Kanzlarich, J. E. Davis, and H. W. H. Lee, Chem. Mater. **8**, 1881 (1996).
16. T. D. Shen, I. Shmagin, C. C. Koch, R. M. Kolbas, Y. Fahmi, L. Bergman, R. J. Nemanich, M. T. McClure, Z. Sitar, and M. X. Quan, Phys. Rev. B **55**, 7615 (1997).
17. D. I. Bilenko, O. Ya. Belobrovaya, É. A. Zharkova, D. V. Terin, and É. I. Khasina, Fiz. Tekh. Poluprovodn. **39**, 834 (2005) [Semiconductors **39**, 800 (2005)].
18. V. P. Tolstoy, I. V. Chernyshova, V. A. Skryshevsky, *Handbook of Infrared Spectroscopy of Ultrathin Films* (New York, Wiley, 2003).
19. T. Arigane, K. Yoshida, T. Wadayama, and A. Hatta, Surf. Sci. **427–428**, 304 (1999).

Translated by A. Kazantsev